JOURNAL OF PROPULSION AND POWER
Vol. 19, No. 4, July–August 2003

Analysis of Inducer Recirculating Inlet Flow

François Bario,* Thierry M. Faure,† and Emmanuel Jondeau‡
École Centrale de Lyon, 69131 Écully Cedex, France
and
Jean-Luc Normand§ and Jean-Michel Nguyen Duc§
SNECMAmoteurs, 27207 Vernon, France

The mean and turbulent features of inducer inlet flow covering various operating points of a centrifugal pump are analyzed. Measurements are conducted in an air test facility with a five-hole pressure probe and an X-wire probe. For flow rates lower than the design flow rate, the recirculation located upstream of the inducer is very strong and creates a global rotation of the fluid from the tip to the hub, upsteam of the inducer. The axial extent of the separated flow decreases as the flow rate increases. The stagnation pressure in this region is higher than the upstream stagnation pressure and can reach several times the inlet dynamic head. In the inlet channel axis, within the recirculated flow, the stagnation pressure is lower than what is found for upstream stations outside the recirculation. This can be related to upstream fluid motion and mixing with the inverse flow, providing stagnation pressure losses. For the flow rates where the recirculation region is large, the incoming flow is deflected toward the hub. Phase-averaged measurements in the inducer inlet show the main time-dependant flow features and their evolution with the flow rate. The analysis shows that, at design and higher flow rates, the evolution of the meridional velocity is correlated with the evolution of the relative flow angle. Relative velocity is not affected by the blade leading edge and is constant at a given radius. The change in the axial velocity is mainly due to the sudden change of the relative flow angle before the blade leading edge.

Nomenclature

D = inlet pipe diameter
h = normalized relative radial position
p = static pressure
p_t = stagnation pressure
Q = flow rate
r = radial coordinate
r_h = hub radius
r_t = tip radius
U = entrainment velocity
V = absolute velocity
V_m = meridional velocity
V_u = tangential velocity
W = relative velocity
z = axial coordinate
α = absolute flow angle
β = relative flow angle
θ = tangential coordinate
ρ = air density
φ = mass flow rate coefficient
ψ_s = static pressure coefficient
Ω = angular velocity

Subscripts

h = hub
t = tip or stagnation
n = design operating point parameter
1 = inlet parameter
2 = outlet parameter

Introduction

INDUCERS have many applications including water jet propulsion, feed systems for rocket pumps, and centrifugal impellers.[1] They are used in the first part of the pump to protect the high-pressure-ratio stages from unsteadiness due to cavitation. The inducer is used to force the collapse of cavitation bubbles into the first part of the pump.[2,3] Thus, the long and narrow passages are designed to increase the stagnation pressure gently and gradually and to avoid cavitation before the main pump.[4] The inducer is also designed to provide a uniform velocity profile to the rotor. Nevertheless, for flow rates lower than the design value, oscillating cavitation can appear and generate shaft vibration,[5] which must be avoided. Increasing tip clearance was found to be effective in preventing rotating cavitation[6] but could not extinguish it. A suction ring, used to control the inlet inverse flow, is very effective in suppressing such cavitation.

Experiments conducted with an air test facility permit the understanding of noncavitating flow behavior. Most of the time, the operating point is selected to avoid a recirculated flow inside the inducer; nonetheless, inlet recirculation can be found during the pump start-up. It has been shown that the cavitation regions are strongly correlated with the recirculating flow.[7] In the past, measurements have underscored the need for a better description of flow patterns in the inducer axial stage inlet.[8] Pump inducer flow is very complex with strong three-dimensional viscous structures developing in the channel due to the very long chord of the inducer blades compared with the channel height (small aspect ratio of the blades). At low flow rates, a separation appears with negative axial flow generally located at the tip of the blade at the inducer inlet. Extensive studies have been conducted on the dynamics of this flow by Janigro and Ferrini[9] and Janigro and Schiavello,[10] who showed the inlet inverse flow or prerotation usually starts at the blade tip and affects various cavitation-related phenomena. These authors suggest that the

Received 23 July 2001; revision received 22 April 2002; accepted for publication 20 May 2002.

*Research Engineer, Laboratoire de Mécanique des Fluides et d'Acoustique, Unité Mixte de Recherche 5509, Centre National de la Recherche Scientifique.

†Assistant Professor, Laboratoire de Mécanique des Fluides et d'Acoustique, Unité Mixte de Recherche 5509, Centre National de la Recherche Scientifique; currently Assistant Professor, Université Pierre et Marie Curie, Paris, 91405 Orsay Cedex, France.

‡Engineer, Laboratoire de Mécanique des Fluides et d'Acoustique, Unité Mixte de Recherche 5509, Centre National de la Recherche Scientifique.

§Engineer, Direction Grosse Propulsion à Liquides.

radial flow may not necessarily be the cause for leakage flow in unshrouded inducers. The recirculation region extends far upstream of the inducer, up to 10 times the inlet diameter.[7] Its induces circumferential and radial velocities in the inlet flow region. Thus, it is important to take recirculation into account for the calculation of the inducer inlet flow. For applications such as rocket pump feed system, where the tank is not far from the inducer, it is possible that this recirculation induces in-block rotation of the fluid in the tank, altering the global behavior of the pump.

Experimental Setup and Apparatus

The experimental setup is an open-circuit facility consisting of an inlet with filters for atmospheric air, a settling chamber followed by the cylindrical inlet duct, the pump that was tested, a vane, a flow meter, and an outlet duct (Fig. 1). The flow is discharged outside the room through the outlet duct. The pump is fitted with a 4-blade inducer, an 8-blade axial–radial shrouded impeller with 8 additional splitters, and an 11-blade diffuser (Figs. 2 and 3). The tip radius r_t is constant from the cylindrical inlet duct to the inducer outlet. The rotational speed is fixed to 5000 ± 10 rpm at standard conditions (inlet pressure 101,325 Pa and temperature 288 K). The origin of the axial direction, $z = 0$, is started at the inducer's tip leading edge. Three flow rates are considered: Q_n (design flow rate), $0.7Q_n$ (reduced flow rate), and $1.3Q_n$ (increased flow rate). The flow rates, corrected for standard conditions, are checked to fall within a 0.6% uncertainty. The Reynolds number for the design condition is 1.78×10^5 and for the investigated flow rates the Reynolds number range varies from 1.24×10^5 to 2.31×10^5.

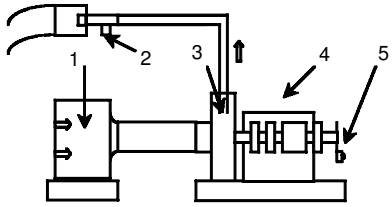

Fig. 1 Schematic view of test rig: 1) inlet settling chamber with dust filter and honeycomb, 2) outlet with venturi and vane, 3) air test pump, 4) electric motor, torque meter, shaft, and bearings, and 5) synchronization device.

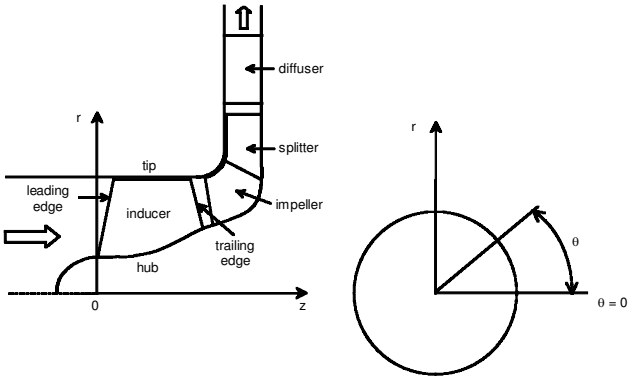

Fig. 2 Schematic of the pump and coordinate system.

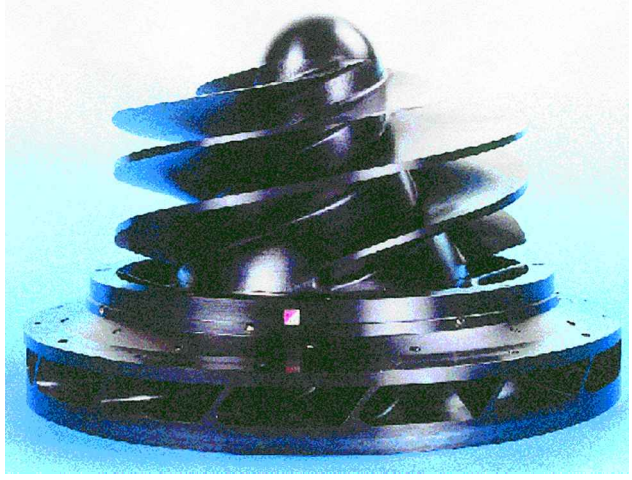

Fig. 3 Experimented inducer.

Seven probe supports on the inlet duct casing wall allow the investigation of velocity and pressure fields, by a directional five-hole probe. The probe diameter is 1 mm and does not perturb the flow. The probe is driven in translation and rotation around its axis by a traversing system. Pressures are measured with differential pressure transducers, giving an accuracy of 10 Pa.

In addition, an X-hot-wire probe was used for instantaneous velocity measurements at a single station upstream of the inducer inlet (plane located at 0.015 inlet diameter of the leading edge of the inducer blade and parallel to it). This probe is calibrated, both in velocity and angle, using the method described by Browne et al.,[11] giving a maximum error of 0.5% for the velocity. Phase averaging of the velocity output was performed with synchronization signal. The instantaneous relative blade position is obtained from the periodic 0–5 V amplitude signal given by the combination of an optical encoder and a toothed wheel placed on the shaft (one pulse per revolution). The probe is aligned with the mean flow obtained from the five-hole pressure probe measurements. The evolution of the tangential and meridional mean and fluctuating velocities over one revolution of the inducer is obtained from the X-hot-wire signals.

Results and Discussion

Overall Performance of the Inducer

The mass flow coefficient is defined as

$$\varphi = Q \Big/ \pi \rho \Omega \left(r_t^2 - r_h^2\right) r_t$$

and the static pressure coefficient by

$$\psi_s = (p_2 - p_1) \Big/ \rho \Omega^2 r_t^2$$

The static pressure performance is shown in Fig. 4. The discontinuity in the curve near $\varphi \sim 0.05$ is due to a higher uncertainty for the lower flow rates. The pump's design value is $\varphi_n = 0.0929$. The curve has a negative slope throughout the flow rates investigated in this study (0.7–1.3 φ_n), and neither surge nor rotating stall occurs.

Upstream Mean Measurements with Five-Hole Pressure Probe

Figure 5 shows the relative radial distribution of the stagnation pressure p_t measured against the atmospheric pressure for several

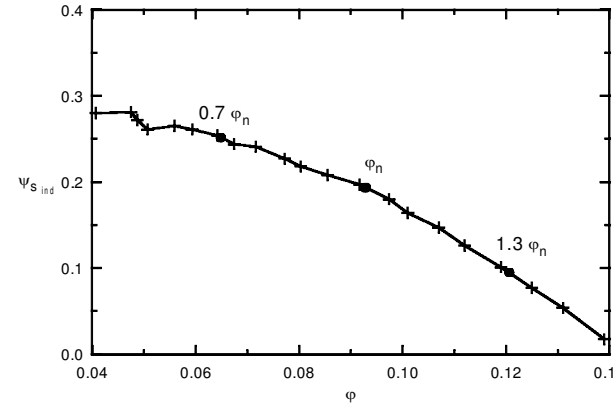

Fig. 4 Static pressure performance of the inducer (ordinate measurement error 10^{-3}).

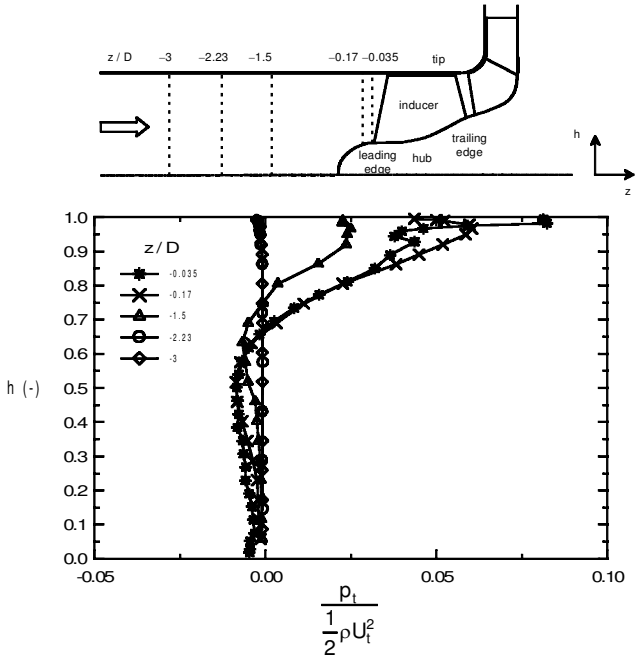

Fig. 5 Relative radial distribution of stagnation pressure upstream from the inducer inlet for $0.7Q_n$ mass flow rate (ordinate measurement error 2×10^{-3}).

axial positions upstream of the inducer and for a flow rate of $0.7Q_n$. The relative radial position is defined as

$$h = (r - r_h)/(r_t - r_h)$$

where r_t and r_h are the tip and hub radius, respectively, with $r_h = 0$ upstream of the pump. The stagnation pressure (measured against the atmospheric pressure) far from the inducer ($z/D = -3$) is constant along the channel height and slightly negative because of stagnation pressure losses in the plenum filter. Near the tip casing, it decreases, showing the viscous effect in the casing boundary layer estimated around 10% of the channel height. Closer to the inducer, the stagnation pressure is negative around $h \sim 0.5$. This negative pressure must be due to losses that are generated upstream of the inducer and can be related to a boundary-layer separation due to the inverse flow with strong energy coming from the inducer. This inverse flow with high tangential and axial velocities in the vicinity of the tip casing acts as a barrier for the incoming axial flow and induces a separation on the casing. This return flow develops radially from the casing into the main flow. Its interaction with the main flow creates important loses through the effect of strong shear forces between the axial main flow and the swirling inverse flow. Figure 5 shows that the negative pressure zone is not attached to the tip casing; nevertheless, its radial development (Fig. 6) occurs over a very short axial distance. The transition region between the low stagnation pressure region ($h < 0.6$) and the inverse flow region where high stagnation pressure is found ($h > 0.9$) corresponds to the flow coming from the inducer and returning toward it through the action of the main incoming flow. According to Yokota et al.,[7] the vortex created in this shear layer area is directly related to the cavitation vortex. The hypothesis of a barrier effect of the swirling inverse flow against the axial incoming flow is verified by the axial velocity plot in the inlet plane (Fig. 6). Near the tip casing, very high levels of absolute stagnation pressure are achieved. This results from flow coming from the inducer. The absolute flow angle, presented in Fig. 7, shows the strong swirl of the inlet flow. In the recirculating area, the flow angle at the tip (varying between -40 deg immediately before the leading edge and -10 deg for the other measurement stations) associated with a high level of absolute velocity (Fig. 8) results because the tangential and axial velocities are very high (Figs. 6 and 9). The thickness of the affected zone is 15% of the channel height at $z/D = -1.5$. The thickness falls to

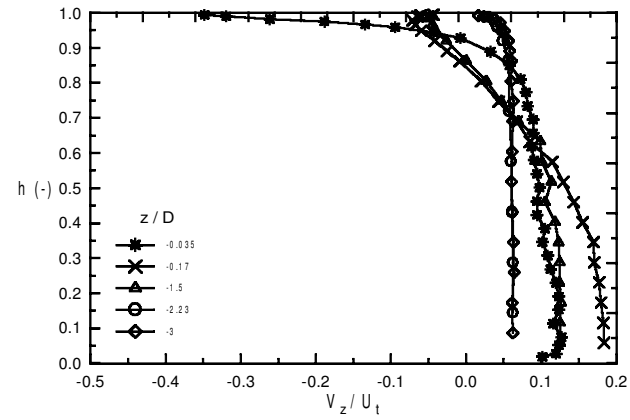

Fig. 6 Relative radial distribution of absolute axial velocity V_z/U_t upstream from the inducer inlet for $0.7Q_n$ mass flow rate (ordinate measurement error 2×10^{-3}).

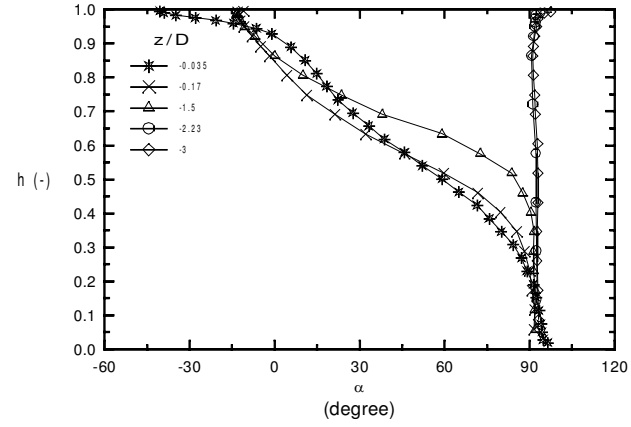

Fig. 7 Relative radial distribution of absolute flow angle α (degree) upstream from the inducer inlet for $0.7Q_n$ mass flow rate (ordinate measurement error 1 deg).

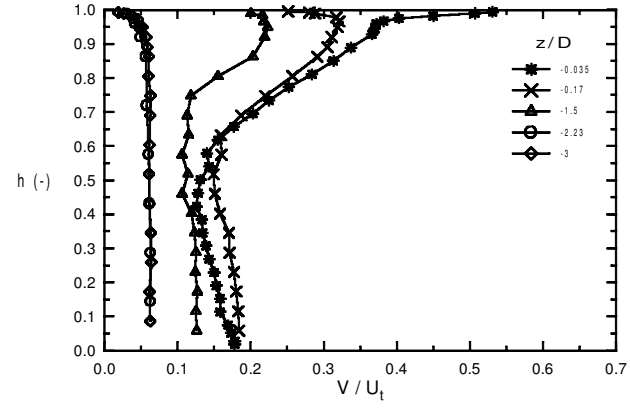

Fig. 8 Relative radial distribution of absolute velocity V/U_t upstream from the inducer inlet for $0.7Q_n$ mass flow rate (ordinate measurement error 2×10^{-3}).

8% immediately before the leading edge ($z/D = -0.035$), but this area is associated with a higher negative axial velocity. Under the momentum balance between the incoming flow and the return flow, there is radial (Fig. 9) and tangential spreading of the inverse flow.

The question that arises is the following: What is the origin of the inverse flow? According to El Ghazzani et al.,[12] the flow exhibits an inviscid vortex coming from the inducer. Near the leading-edge blade tip, because of the camber and shape of the leading edge (from hub to tip), the streamlines on the pressure side are deflected toward

the low-pressure area, that is, toward and upstream the tip. On the suction side, the streamlines are deflected toward and downstream the hub. This purely inviscid explanation of the phenomenon is validated by three-dimensional Euler calculations on the LH2 pump of the Vulcain engine of Ariane V.[12] This vortex is not related to the tip leakage vortex mentioned by Del Valle et al.[13] or Bhattacharyya et al.[14] because the inviscid calculation of El Ghazzani et al.[12] is done without tip leakage. It is a fully three-dimensional effect, strongly coupled with the incidence effect along the leading-edge span. The fact that recirculating flow is not generated in the tip leakage flow is also confirmed by the experimental study of Offtinger et al.[15] They compare the flow of an unshrouded inducer and the flow of the same inducer with a shroud. The difference between the two tangential and axial velocity distributions upstream of the inducers at low mass flow rate is small. The effect of the removal of the shroud is a slight increase of the absolute flow angle; there is no change in the global evolution of the flow. Although this vortex origin maybe inviscid, this high-energy vortex with strong tangential velocity and high resulting absolute stagnation pressure interacts with other vortices, such as the tip leakage vortex and casing boundary-layer vortices, where

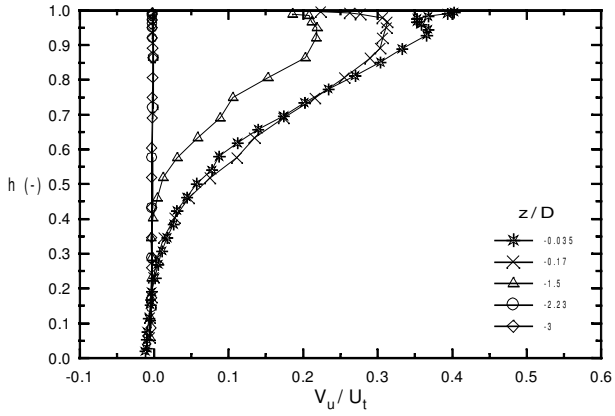

Fig. 9 Relative radial distribution of absolute tangential velocity V_u/U_t upstream from the inducer inlet for $0.7Q_n$ mass flow rate (ordinate measurement error 2×10^{-3}).

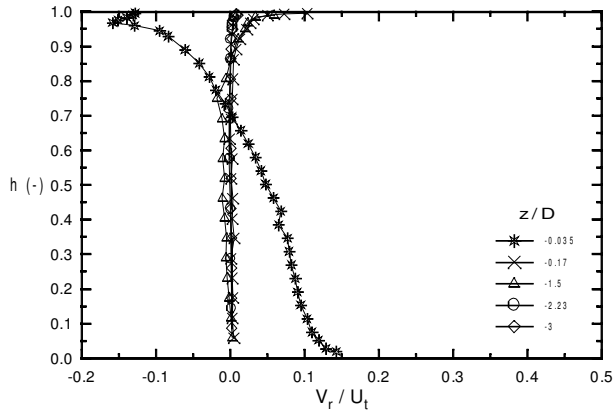

Fig. 10 Relative radial distribution of absolute radial velocity V_r/U_t upstream from the inducer inlet for $0.7Q_n$ mass flow rate (ordinate measurement error 2×10^{-3}).

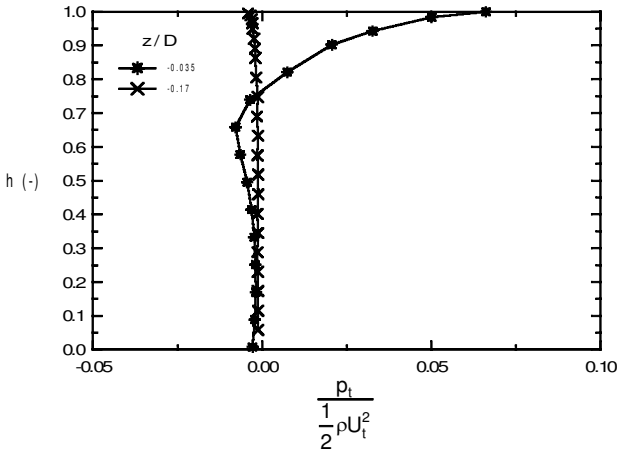

Fig. 11 Relative radial distribution of stagnation pressure upstream from the inducer inlet for $0.9Q_n$ mass flow rate (ordinate measurement error 2×10^{-3}).

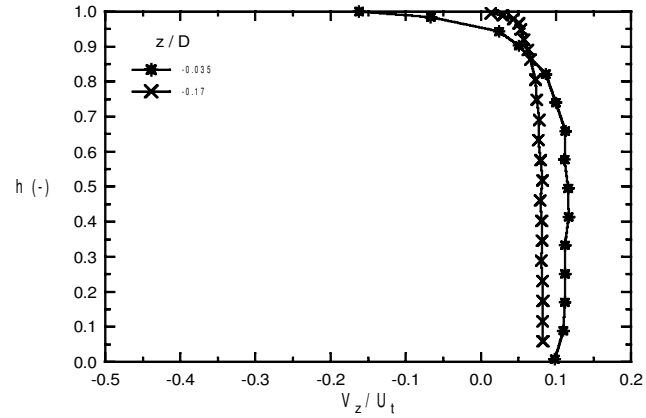

Fig. 12 Relative radial distribution of absolute axial velocity V_z/U_t upstream from the inducer inlet for $0.9Q_n$ mass flow rate (ordinate measurement error 2×10^{-3}).

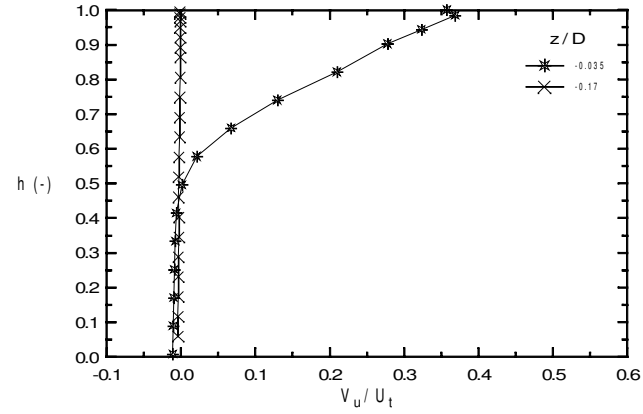

Fig. 13 Relative radial distribution of absolute tangential velocity V_u/U_t upstream from the inducer inlet for $0.9Q_n$ mass flow rate (ordinate measurement error 2×10^{-3}).

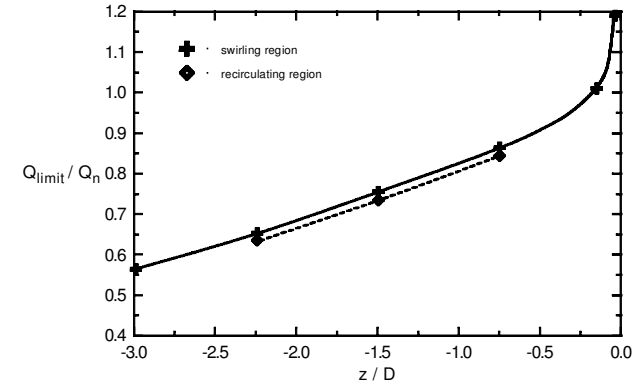

Fig. 14 Evolution of the length of the recirculated flow with the flow rate.

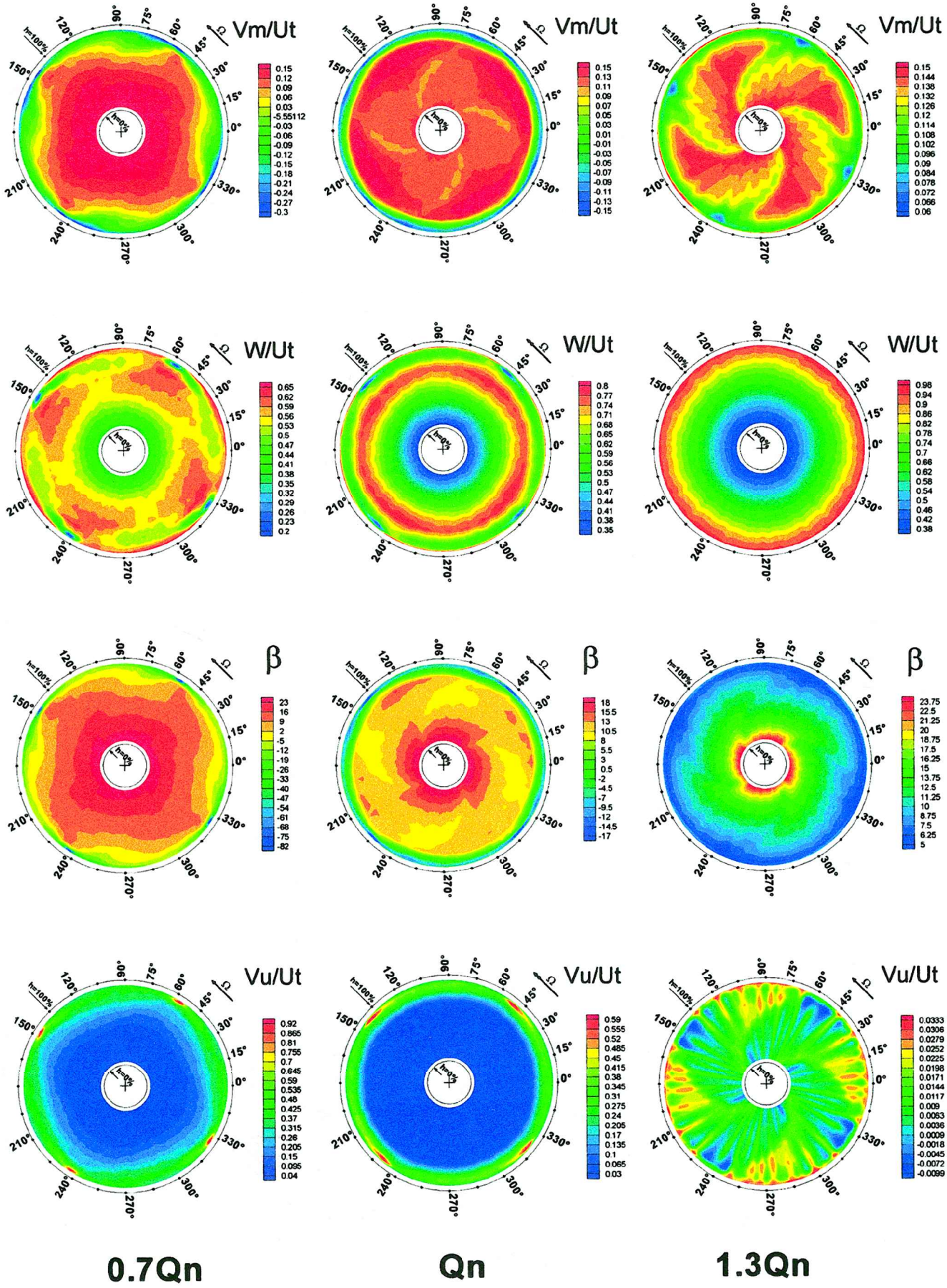

Fig. 15 From top to bottom, meridional and relative velocity, relative flow angle and tangential velocity for three flow rates (from left to right, $0.7Q_n$, Q_n, and $1.3Q_n$).

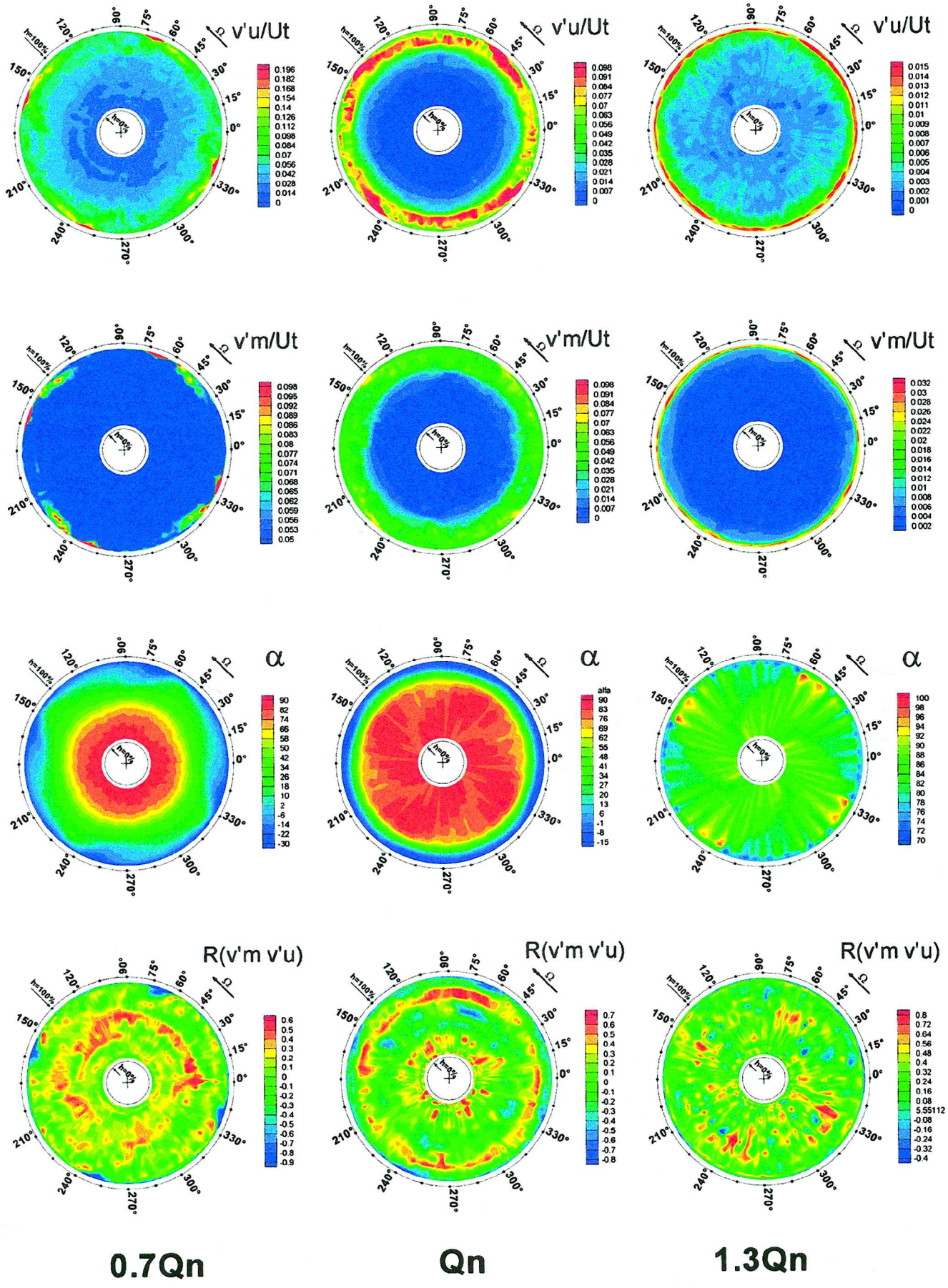

Fig. 16 From top to bottom, standard deviations of tangential and meridional velocity fluctuations, absolute flow angle, and cross-correlation coefficient for three flow rates (from left to right, $0.7Q_n$, Q_n, and $1.3Q_n$).

viscous effects are dominant. For these reasons many authors impute the origin of the recirculating flow to the tip leakage flow.

The velocity distribution (Fig. 8) exhibits a constant value, except in the boundary layers, for stations $z/D = -2.23$ and $z/D = -3$. For $z/D = -1.5$, the increase in the tangential velocity everywhere inside the channel is due to the viscous effect of the inducer's rotation. This rotation increases near the inducer inlet. The radial velocity distribution is almost constant except in the casing vicinity for all of the profiles (Fig. 10) not immediately upstream of the leading edge. A radial gradient from root to tip appears for $z/D = -0.035$ and is caused by the strong vertical motion of the inducer suction. Similar comments are valid for flow rates greater than $0.7Q_n$, the recirculation length decreasing with increasing flow rate. Note that in Figs. 11–13, for $0.9Q_n$, there is no evolution upstream of $z/D = -0.17$.

Extent of Recirculating and Swirling Zones

Figure 14 shows the limit flow rate corresponding to the beginning of the recirculating and swirling regions as a function of the axial position of the measurement. The recirculation limit corresponds to the location where the first zero axial velocity is found near the casing. The swirling limit corresponds to the location where induced tangential velocities are found without negative axial velocity near the casing. For that, a probe is put near the casing and aligned with the axial direction. The flow rate is varied from high values to low values. The probe accuracy is defined to ± 2 deg; thus, if a 2-deg change is found at a given flow rate, then it is considered the limit of an induced tangential velocity. This measurement is repeated for the seven axial locations of the probe. As mentioned earlier, the extent of the swirling region along the radius is greater than the extent of the recirculating region. The difference of the axial extent between these two zones at the tip casing is small. For $0.7Q_n$, the swirling zone extends up to 1.85 inlet diameters upstream of the inducer. Very close to the inducer leading edge, recirculation region exists up to $1.2Q_n$. The extrapolation of Fig. 14 for $0.4Q_n$ yields a swirling zone extending 4–5 inlet diameters upstream of the inducer.

Upstream Measurements with X-Wire Probe

Polar plots of phase-averaged mean velocities, standard deviation of fluctuating velocities, and phase-averaged flow angles are shown in Figs. 15 and 16 for a station immediately upstream of the inducer leading edge. Three operating points are presented: From left to the right, Figs. 15 and 16 show results for the low flow rate $0.7Q_n$, the design flow rate Q_n, and the high flow rate $1.3Q_n$, respectively. To show the different flow features, the scaling is not the same for the three flow rates.

At $1.3Q_n$, the meridional velocity V_m shows that there is no mean or local negative meridional velocity in the measurement plane. The four blades and the shape of the leading edge are clearly identified as a velocity defect. At the tip, four spots of low meridional velocity are found at $\theta = 65, 155, 245, 335$ deg. They are directly connected with four spots of low relative flow angle β. There are no corresponding spots of low relative velocity W. The W velocity plot shows rings of equal level regions, with increasing velocity from root to tip. In the entire flowfield, the tangential gradients of the meridional velocity V_m are not correlated to relative velocity W gradients but to relative flow angle β gradients. In other words, at this station, the relative velocity does not decrease when the relative flow reaches the leading edge of the inducer. There is no blockage effect in terms of relative velocity reduction. The tangential velocity shows the four blades shapes with a modulation probably induced by information coming from downstream. The change of the meridional velocity is only related to the change of direction of the relative velocity. This is also clearly visible for the nominal mass flow rate $Q = Q_n$. At this flow rate, a quasi-circular ring of negative meridional velocity V_m is found at the tip. The width of the recirculating region attached to the casing is 8–10% of the channel height, depending on the azimutal location considered. The tangential velocity V_u and the absolute flow angle α (Figs. 15 and 16) show that the rotation of the fluid is important and affects the whole flow field, not only the recirculating region. Four spots of high tangential velocity V_u located at the tip at $\theta = 50, 140, 230, 320$ deg are found. Except for these regions, the tangential velocity distribution is axisymetric.

At the lower flow rate $0.7Q_n$, the meridional velocity shows a higher gradient in the circumferential plane. The width of the recirculating region is 8–20% of the channel height depending on the azimutal location and is larger in the vicinity of the blade tip. These regions with high relative velocities can be considered similar to the core at the blade passage vortex described by Lashminarayana.[1] The fluctuations of the tangential velocity are stronger than the fluctuations of the meridional velocity. Near the blade tip, very high fluctuations are observed for the tangential velocity in Fig. 16. The highest value of the tangential fluctuation is found in the zones with the highest tangential velocity corresponding to the lower relative velocity region. This zone is located at the tip at $\theta = 50, 140, 230, 320$ deg for the nominal mass flow rate and at $\theta = 58, 148, 238, 328$ deg at $0.7Q_n$. This difference is due to the larger value of the tangential velocity: At the measurement location, the rotation of the flow in the absolute frame is larger for the lower mass flow, and so this zone is found at a higher azimutal location. The turbulent shear stress (the ratio of the shear stress to the product of the tangential and axial fluctuating velocity in Fig. 16) is very high at the border of the recirculating flow. This border is the starting point of cavitation in the inducer of a liquid pump.[7] For the higher mass flow $1.3Q_n$, as mentioned before, there is no inverse flow, particular flow features are observed in the tangential velocity and absolute flow angle plots. A modulation of these quantities is found probably induced by information coming from the impeller.

Conclusions

Measurements have been performed with five-hole pressure probes and hot-wire at the inlet and immediately upstream of the leading edge of a four-blade inducer. Classical results concerning inducer recirculating flows are found.

1) The tip casing shows high stagnation pressures. The stagnation pressure becomes negative at midchannel. This negative pressure is probably due to losses that are generated upstream of the inducer and can be linked to boundary-layer separation due to inverse flow induced by the inducer. This inverse flow with high tangential and axial velocities in the tip casing vicinity acts as a barrier for the axial incoming flow.

2) The axial length of the swirling zone (rotation of the fluid without inverse flow) is greater than the extent of the inverse flow. The zone of high stagnation pressure is greater than the recirculation zone.

3) The recirculating flow is not generated in the tip leakage flow; it is a fully three-dimensional effect strongly coupled with the incidence effect along the leading-edge span and is mainly in the tip region.

4) The tangential gradients of the axial velocity are not correlated to relative velocity gradients but to relative flow angle gradients: The relative velocity does not decrease when the relative flow reaches the leading edge of the inducer.

5) There is no blockage effect in terms of relative velocity reduction. The change of the axial velocity is only related to the change of direction of the relative velocity.

6) Phase-averaged turbulent measurements have been conducted immediately upstream of the inducer to address the questions about time-dependant flow features. The standard deviations of the fluctuations for tangential velocity are stronger than for the meridional velocity, particularly near the casing. Information from the impeller and the downstream diffuser may affect the flow for this section at the $1.3Q_n$ flow rate.

Acknowledgments

The authors would like to thank the Centre National d'Études Spatiales and the Société Nationale d'Études et de Construction de Moteurs d'Aviation for financial support of this study. The help of V. C. Sharma for the text revision is gratefully acknowledged.

References

[1]Lakshminarayana, B., "Fluid Dynamics of Inducers—A Review," *Journal of Fluids Engineering*, Vol. 104, No. 4, Dec. 1982, pp. 411–427.

[2]Boccazzi, A., Perdichizzi, A., and Schiavello, B., Tabacco, U., "Cavitation Behaviour and Internal Flow Measurements by Laser Doppler Anemometry in a Low Solidity Inducer," XXèmes Journées de l'Hydraulique, Société hydrotechnique de France, Rept. 16, 4–6 April 1989.

[3]Boccazzi, A., Perdichizzi, A., and Tabacco, U.,"Flow Field Investigation in a Low Solidity Inducer by Laser Doppler Velocimeter," *Journal of Turbomachinery*, Vol. 112, No. 1, Jan. 1990, pp. 91–97.

[4]Lakshminarayana, B., *Fluid Dynamics and Heat Transfer of Turbomachinery*, Wiley, New York, 1996, pp. 131–142.

[5]Tsujimoto, Y., Yoshida, Y., Maekawa, Y., Watanabe, S., and Hashimoto, T., "Observations of Oscillating Cavitation of an Inducer," *Journal of Fluids Engineering*, Vol. 119, No. 4, Dec. 1997, pp. 775–781.

[6]Kamijo, K., Yoshida, M., and Tsujimoto, Y., "Hydraulic and Mechanical Performance of LE-7 LOX Pump Inducer," *Journal of Propulsion and Power*, Vol. 9, No. 6, 1993, pp. 819–826.

[7]Yokota, K., Kurahara, K., Kataoka, D., Tsujimoto, Y., and Acosta, A. J., "A Study of Swirling Backflow and Vortex Structure at the Inlet of an Inducer," *Japanese Society of Mechanical Engineers International Journal*, Series B, Vol. 42, No. 3, 1999, pp. 451–459.

[8]Bario, F., Barral, L., and Bois, G., "Air Test Flow Analysis of the Hydrogen Pump of Vulcain Rocket Engine," *Journal of Fluids Engineering*, Vol. 113, No. 4, Dec. 1991, pp. 654–659.

[9]Janigro, A., and Ferrini, F., "Inducer Pumps," *Recent Progress in Pump Research*, von Kármán Inst. Lecture Series 61, Rhode St. Genèse, Belgium, Vol. 1, 1973, pp. 1–113.

[10]Janigro, A., and Schiavello, B., "Prerotation in Centrifugal Pumps. Design Criteria," *Off-Design Performance of Pumps*, von Kármán Inst. Lecture Series 1978-3, Rhode St. Genèse, Belgium, 1978.

[11]Browne, L. W. B., Antonia, R. A., and Chua, L. P., "Calibrating of X-probes for Turbulent Flow Measurements," *Experiments in Fluids*, Vol. 7, No. 3, 1989, pp. 201–208.

[12]El Ghazzani, M., Bois, G., Geai, P., and Lebœuf, F., "Three-Dimensional Inviscid Flow Computations in a Spatial Turbopump Inducer Using a Distributed Loss Model," American Society of Mechanical Engineers, ASME Paper 92GT65, June 1992.

[13]Del Valle, J., Braisted, D. M., and Brennen, C. E., "The Effects of Inlet Flow Modification on Cavitating Inducer Performance," *Journal of Turbomachinery*, Vol. 114, No. 2, April 1992, pp. 360–365.

[14]Bhattacharyya, A., Acosta, A., Brennen, C., and Caughey, K., "Observations on Off-design Flows in Non-cavitating Axial Flow Inducers," *Pumping machinery*, FED Vol. 154, American Society of Mechanical Engineers, Fair field, NJ, 1993, pp. 135–141.

[15]Offtinger, C., Henry, C., Morel, R., and Spettel, F., "Experimental Comparison of Flow Fields at the Inlet and the Outlet of an Inducer With Shrouded and Unshrouded Configurations," *Journal of Fluids Engineering*, Vol. 119, No. 4, Dec. 1997, pp. 954–959.